RESEARCH PAPER

ice | science

ICE SCIENCE – Keywords
Hydration; Rietveld Method; Backscattered Electron Imaging; Compressive Strength; Sulfobelite.

Hydration of Belite-Ye'elimite-Ferrite(BYF) cements with different calcium sulfate sources

Gema Álvarez-Pinazo, Dr.
X-Ray Data Services S.L., Edificio GREEN RAY, 1ª planta, Avda. Louis Pasteur, 47 (Ampliación Campus Teatinos), 29010-Málaga, Spain
Departamento de Química Inorgánica, Cristalografía y Mineralogía, Universidad de Málaga, 29071-Málaga, Spain
Isabel Santacruz, Dr.
Departamento de Química Inorgánica, Cristalografía y Mineralogía, Universidad de Málaga, 29071-Málaga, Spain
Miguel A. G. Aranda. Professor.
Departamento de Química Inorgánica, Cristalografía y Mineralogía, Universidad de Málaga, 29071-Málaga, Spain
CELLS-Alba Synchrotron, Carretera BP 1413, Km. 3.3, E-08290 Cerdanyola, Barcelona, Spain
***Ángeles G. De la Torre,** Dr.
Departamento de Química Inorgánica, Cristalografía y Mineralogía, Universidad de Málaga, 29071-Málaga, Spain
Tel.: +34952131877; fax: +34952132000. E-mail address: mgd@uma.es

Abstract

Belite-Ye'elimite-Ferrite cements, BYF, are a sustainable alternative to OPC to reduce CO_2 emissions. The aim of this research is to understand the influence of the sulfate source on the hydration of two laboratory-prepared BYF-cements. One studied clinker contained β-belite and orthorhombic-ye'elimite (non-active), and the other one α'_H-belite and pseudo-cubic-ye'elimite (activated with borax during clinkering). Pastes were mainly characterized through Rietveld-quantitative-phase-analysis of powder patterns, thermal analysis and scanning-electron-microscopy. Active-mortars developed higher compressive strengths than non-active-mortars, independently of the sulfate source. The highest values for active-mortars (w/c=0.55) were 40±1MPa (28d) with anhydrite, and 68±1MPa (120d) with gypsum.

1. Introduction

Cement manufacturing is an industry that consumes a large amount of energy and emits a great deal of CO_2. For every ton of ordinary Portland cement (OPC) produced, 0.54 tons of CO_2 are released into the atmosphere because of the decomposition of calcite in the kilns. On average, 0.34 and 0.09 tons of CO_2 are also emitted due to fuel and electricity consumption, respectively (Van Oss and Padovani, 2003; Hasanbeigi et al., 2010). Some studies have estimated that the cement industry contributes around 6% of all anthropogenic CO_2 emissions (Flatt et al., 2012; Gartner, 2004). In recent times a lot of attention has been paid to the development of some modified special cement clinkers, leading to energy saving and CO_2 emission reduction. A possibility to reduce the environmental impact of cement production is the use of low-calcite-demanding cements (Gartnet, 2004). Some of these binders are based on belite (C_2S) or ye'elimite ($C_4A_3\bar{S}$), which is also called Klein's salt. Belite-Ye'elimite-Ferrite (BYF), previously known as Calcium SulfoAluminate or sulfobelite cements (Garnet and Hirao, 2015; Li and Gartner, 2006; Cuberos et al., 2010), have belite as the main phase, and ye'elimite as a second component; they have been proposed as an alternative binder to reduce CO_2 emissions in the cement clinker production because these materials require both lower amounts of limestone and lower operating temperatures and, in addition, they are easily ground. Because of that, the CO_2 footprint of sulfobelite cements is about 30% lower than that for OPC. The most common composition of BYF clinkers includes β-C_2S, $C_4A_3\bar{S}$ and C_4AF, being iron-rich sulfobelite materials (Álvarez-Pinazo et al., 2013), recently named as BYF (Garnet and Hirao, 2015). An industrial trial to produce around 2500 tons of BYF was carried out in early 2011 by Lafarge under the AETHER^{TM} project (http://www.aether-cement.eu (Walenta and Comparet, 2011).

BYF cements are prepared by grinding the clinker with different amounts of a calcium sulfate set regulator such as gypsum, bassanite or anhydrite. These systems are complex and there are many parameters affecting the hydration mechanism (Aranda and De la Torre, 2013), such as type and amount of sulfate source

(Allevi et al., 2004; Pera and Ambroise, 2004), belite and ye'elimite polymorphism (Cuesta et al., 2014), the presence of minor phases, water/solid ratio, and so on. The water demand needed for a complete hydration process is determined by the amount of calcium sulfate and silicates, and is slightly higher than that for OPC (for complete hydration). Larger water-to-cement (w/c) ratios led to smaller strength developments and also may modify the hydration reactions. In any case, and as today, researchers dealing with BYF have reported a wide range of w/c ratios usually spanning between 0.35 and 0.65.

During early age hydration, ettringite or AFt ($C_6A\bar{S}_3H_{32}$) phase is the main crystalline hydration product together with amorphous aluminum hydroxide (amorphous-AH_3). Ettringite is formed in these cements from the dissolution of ye'elimite and calcium sulfate (gypsum, bassanite or anhydrite) according to Eq. (1). Once the sulfate source is depleted and if there is enough water available, monosulfate ($C_4A\bar{S}H_{12}$), which is an AFm-type phase, and hereafter will be labeled as AFm, is formed according to Eq. (2) (Winnefeld and Lothenbach, 2010). However, there are some contradictory results concerning the reactivity of ye'elimite with water in the absence of another sulfate source. Some authors stated that only reaction (2) takes place (Winnefeld and Barlag, 2010) while others have published that mixtures of AFt and AFm phases are produced (Álvarez-Pinazo et al., 2014; Berger et al., 2011).

$$C_4A_3\bar{S} + 2\,CH_x + (38-2x)\,H \rightarrow C_6A\bar{S}_3H_{32} + 2\,AH_3 \quad (x = 0, 0.5 \text{ or } 2) \qquad (1)$$

$$C_4A_3\bar{S} + 18\,H \rightarrow C_4A\bar{S}H_{12} + 2\,AH_3 \qquad (2)$$

Recently new data on the mechanisms for the early age hydration of ye'elimite have been published (Cuesta et al., 2014). This study demonstrated that hydration kinetics not only depend on the w/c ratio and the solubility of the additional sulfate source, but also on the polymorphism of ye'elimite and the presence of foreign ions incorporated into the crystal structure of ye'elimite.

Furthermore, the hydration kinetics of belite is highly depending on its polymorphism. Thus, α-forms of belite are considered more reactive than β-C_2S (Chatterjee, 1996). Nevertheless, it should be noted that the presence of sulfate(Gies and Knofel, 1987; Martín-Sedeño et al., 2010) or different ions (B_2O_3, Na_2O, K_2O, BaO, MnO_2, Cr_2O_3 or their combinations) (Kantro and Weise, 1979; Matkovic et al., 1981; Fierens and Tirlocq, 1983; Ziemer et al., 1984; Benarchid et al., 2004) in the belite structure, can promote the formation of α'_H-C_2S and increase its hydraulic properties (Bensted, 1979; Fukuda et al., 2001). Also the chemical environment (high or low available amorphous aluminum hydroxide content) may have some influence on the belite reactivity. Independently of the kinetic of the reaction, C_2S may yield stratlingite (C_2ASH_8) or amorphous C-S-H gel and portlandite (CH). These two alternative chemical processes can be expressed as the following Eqs.:

$$C_2S + AH_3 + 5\,H \rightarrow C_2ASH_8 \qquad (3)$$

$$C_2S + (2-x+y)\,H \rightarrow C_xSH_y + (2-x)\,CH \qquad (4)$$

Finally, the reactivity of ferrite (C_4AF) during hydration in these cements is slower than that of $C_4A_3\bar{S}$ and it is still not well understood. The hydration process involving iron-containing phases is very complex, because the formation of solid solutions between Fe- and Al-containing hydrates may stabilize mixed solids, such as Fe-rich AFt (Möschner et al., 2009) and Fe-rich AFm (Dilnesa et al., 2012). Moreover, if the calcium concentration increases, ferrite phase can take part of the formation of katoite or siliceous hydrogarnet by the following Eq. (Álvarez-Pinazo et al., 2014):

$$C_2S + x\,C_4AF + 10x\,H \rightarrow C_3A_{1-x}F_xSH_4 + (4x-1)\,CH + (2x-1)\,AH_3 \quad (0.5<x<1.0) \qquad (5)$$

In our system, the presence of different polymorphs of ye'elimite and belite affects the hydration due to the different reactivity of those phases. The aim of this study is to understand the influence of different types of calcium sulfate sources on the hydration of two laboratory-prepared BYF cements which contain different belite (β-C_2S or α'_H-C_2S) and ye'elimite (orthorhombic or pseudo-cubic) polymorphs. Pastes were characterized through laboratory X-ray powder diffraction, rheological measurements, scanning electron microscopy and thermogravimetric analyses. Finally, the compressive strength values of the corresponding mortars were also measured and the role of the sulfate source is discussed.

2. Materials and methods

2.1. Materials

Two laboratory BYF clinkers (labeled as B0 and B2), prepared as previously reported (Álvarez-Pinazo et al., 2012), have been used. The expected phase composition was 50 wt% C_2S, 30 wt% of $C_4A_3\bar{S}$ and 20 wt% of C_4AF. B2 clinker was prepared by adding to raw materials 2 wt% expressed as B_2O_3 of borax. The raw materials were heated at 1350ºC during 30 min (heating rate of 5 ºC/min) and finally quenched with air flow. The clinkered pellets were grinded in the micro-Deval mill at 100 rpm for 1 hour. B0 clinker (non-active) contains β-C_2S and orthorhombic ye'elimite as main phases, meanwhile α'_H-C_2S and pseudo-cubic ye'elimite are stabilized in B2 clinker due to the addition of borax to the raw mixture (active clinker) (Álvarez-Pinazo et al., 2012). Commercial micronized natural gypsum, $C\bar{S}H_2$, marketed by

BELITH S.P.R.L. (Belgium), was also used as a raw material. Rietveld quantitative phase analysis (RQPA) of gypsum was performed, obtaining 94.5(2) wt% of $C\bar{S}H_2$, 2.6(1) wt% of insoluble-$C\bar{S}$, 2.2(1) wt% of $SrSO_4$ and 0.6(1) wt% of Na_2SO_4. Bassanite ($C\bar{S}H_{0.5}$) and anhydrite ($C\bar{S}$) were synthesized by heating natural gypsum at 90ºC for 24 h in a stove and at 700ºC for 1 h in a furnace, respectively. Clinkers were mixed with 10 wt% of each of the three different sulfate sources to obtain different cements, named hereafter as X10Bx, where X can be gypsum (G), bassanite (B) or anhydrite (A), and x can be either 0 or 2 (for non-active or active clinkers, respectively). Due to the different water content of sulfate sources, the total amounts of SO_3 in the cements are slightly different and are included in Table 1.

2.1.1. Preparation of cement pastes.

All cement pastes were prepared with distilled water, w/c=0.55. Taking into account the amount of water in the sulfate sources, the real w/c ratios were 0.58, 0.56 and 0.55, for G10Bx, B10Bx and A10Bx, respectively. These pastes were mixed in an agate mortar and immediately introduced into a hermetically closed polytetrafluoroethylene (PTFE) cylinder mold during the first 24 hours at 20±1ºC (García-Maté et al., 2015). Then, samples were taken out and stored within deionized water at 20±1°C. Pastes were characterized after 3, 7, 28, 120, 180 and 365 days of hydration. A small amount (0.05 wt% of active matter referred to total solids content) of a commercial polycarboxylate-based superplasticizer (SP), Floadis 1623 (Adex Polymer S.L., Madrid, Spain), with 25 wt% of active matter, was added to water to prepare bassanite-pastes that show similar rheological behavior than those prepared with gypsum or anhydrite.

2.1.2. Stopping hydration of pastes.

At the selected curing ages, pastes were milled into fine powder in an agate mortar prior to stopping hydration. The stopping procedure consisted on washing twice with acetone (Prolabo S.A.) in a Whatman filtration system (70 mm diameter Whatman filter with a pore size of 2.5 μm and a Teflon support) and finally with diethyl ether (Prolabo S.A.) (Odler and Abduk-Maula, 1984). The obtained powder was divided into two fractions to perform laboratory X-ray diffraction and thermal characterization. The former was stored in a desiccator with silica gel and KOH to avoid further hydration or carbonation (García-Maté et al., 2013; Wang, 2010).

2.2. Analytical techniques

2.2.1. Laboratory X-Ray Powder Diffraction (LXRPD).

LXRPD studies were performed on both anhydrous and stopped-hydration samples cured for 3, 7, 28, 120, 180 and 365 days. In order to evaluate the Amorphous and Crystalline non-quantified (ACn) content, an external standard approach was employed (Jansen et al., 2011; O`Connor and Raven, 1998; Cline et al., 2011). Patterns were recorded in Bragg-Brentano reflection geometry ($\theta/2\theta$) on an X'Pert PRO MPD diffractometer (PANalytical B.V.) using strictly monochromatic CuKα_1 radiation (λ=1.54059Å) [Ge (111) primary monochromator]. The X-ray tube worked at 45 kV and 40 mA. The optics configuration was a fixed divergence slit (1/2°), a fixed incident antiscatter slit (1°), a fixed diffracted anti-scatter slit (1/2°) and X'Celerator RTMS (Real Time Multiple Strip) detector, working in scanning mode with maximum active length. Data were collected from 5º to 70° (2θ) for ~2 hours. The samples were rotated during data collection at 16 rpm in order to enhance particle statistics.

The external standard (a polished polycrystalline quartz rock placed on the diffractometer in the very same orientation each measurement) pattern was collected in identical diffractometer configuration/conditions (except for the spinning rate of the sample) and as close in time as possible to the pastes measurements to determine a diffractometer constant (G-factor) (Jansen et al., 2011; O`Connor and Raven, 1998). The suitability of this quartz-rock was tested against NIST standard reference material SRM-676a (α-Al_2O_3) (Cline et al., 2011).

2.2.2. LXRPD data analysis.

LXRPD patterns of anhydrous cements, stopped-hydration pastes and the external standard were analyzed by the Rietveld methodology as implemented in the GSAS software package (Larson and Von Dreele, 2004) to extract the RQPA (De la Torre et al., 2001) and ACn contents by external methodology (Aranda et al., 2012). The refined overall parameters were phase scale factors, background coefficients, unit cell parameters, zero-shift error, peak shape parameters, and preferred orientation coefficient, if needed. March-Dollase ellipsoidal preferred orientation algorithm was employed (Dollase, 1986). Peak shapes were fitted by using the pseudo-Voigt function (Thompson and Cox, 1987) including the asymmetry correction (Finger et al., 1994).

2.2.3. Rheological behavior.

Prior to rheological characterization, pastes were prepared by mechanical stirring according to EN196-3:2005 standard procedure. Rheological measurements of fresh pastes were carried out using a viscometer (Model VT550, Thermo Haake, Karlsruhe, Germany) with a serrated coaxial cylinder sensor, SV2P, provided with a solvent trap to reduce evaporation. Flow curves were obtained under controlled rate (CR) measurements. Ramp times of 6 s were recorded in the shear rate range between 2 and 100 s^{-1} for a total of 12 ramps. A further decrease from 100 to 2 s^{-1} shear rate was performed by following the same ramp times. Prior to the rheological measurement, pastes were pre-

sheared for 30 s at 100 s^{-1} and held at 0 s^{-1} for 5 s in the viscometer.

2.2.4. Thermal analysis.

Differential thermal (DTA) and thermogravimetric (TG) analyses were performed in a SDT-Q600 analyzer from TA instruments (New Castle, DE) for a ground fraction of every paste after stopping hydration as described above. The temperature was varied from room temperature (RT) to 1000°C at a heating rate of 10 °C/min. Measurements were carried out in open platinum crucibles under nitrogen flow. The weighed loss from RT to 600°C was assumed to be water (free and chemically bounded water) and that from 600 to 1000°C was considered as CO_2.

2.2.5. Specific surface area determination (BET).

The specific surface area of anhydrous cements was carried out in an automatic MICROMERITICS ASAP 2020, and was determined by BET (Brunauer-Emmett-Teller) method. Isotherms at low partial pressures of the inert gas (N_2, at 77K) were used to determine specific surface areas, by assuming that molecules of the sorbate are adsorbed on surfaces that can include the walls of pores, provided that the distance between molecules on opposing walls is large compared with molecular dimensions. The BET method gives results two to three times higher than the air permeability values (Blaine method) because it includes internal surfaces present in microcracks or in pores open at only one end.

2.2.6. Scanning Electron Microscopy (SEM).

The microstructure of selected pastes was observed in a JEOL JSM-6490LV scanning electron microscope with the backscattered electron mode (BSE) working at 20 kV acceleration voltage. At the selected ages (7 and 120 days), a slice of the samples was cut from the cylinder and the hydration was stopped by immersing them in isopropanol for 3 days and then heated at 40°C for 24 hours. After that, samples were impregnated with a low viscosity resin, polished using diamond spray (down to 1 µm) and sputtered with graphite prior to SEM observations. The chemical analyses were carried out with the OXFORD INCA Energy 350 energy dispersive spectrometer.

2.2.7. Compressive strength.

Standard mortars were prepared with active and non-active BYF cement/sand/water ratio of 1/3/0.55 following the European standard EN196-1 using standard sand. Cubic samples of 30×30×30 mm were prepared by casting the mortar in a jolting table (Model UTCM-0012, 3R, Montauban, France) with a total of 120 knocks. For a better homogenization, molds were half cast and knocked during 60 times. After that, they were fully cast and other 60 knocks were performed. The compressive strength values of these mortars (at 3, 7, 28 and 120 days of hydration) were measured according to the European standard EN196-1 in a compression press (Model Autotest 200/10 W, Ibertest, Madrid, Spain) at the rate of 1.5 MPa·s^{-1}; the reported values are the average of three broken cubes. The measured compressive strength values were corrected by a factor of 1.78 to take into account the difference in area with standard prisms (40×40×160 mm). This factor is obtained by dividing the compression area of the machine (1600 mm2) by the specimen area (900 mm2).

3. Results and discussion

3.1. Rheological characterization of the pastes

Bassanite dissolves quicker in water than gypsum or anhydrite. In addition, bassanite in contact with water suffers from a fast grain decay (intergranular attack) which produces an increasing of the surface area of the sulfate carrier, and as a consequence, a high water demand (and high viscosity). In addition, a primary gypsum precipitation occurs (García-Maté et al., 2015), which will also affect the rheological behavior of the paste. Thus, both parameters the high water demand and the gypsum precipitation increase the viscosity of bassanite-pastes. Consequently, the addition of SP may well be useful to reduce the viscosity.

Figure 1 shows the flow curves of X10B2 pastes. The bassanite-containing paste shows the highest viscosity values and hysteresis cycle (the latter may be something reversible, and it is related to a fast setting), in agreement with previous studies (García-Maté et al., 2015). Since our objective is to study the effect of the calcium sulfate source including compressive strengths of the corresponding mortars, similar rheological behavior, and in particular, similar viscosity values at very early hydration ages are desired. When a small amount of SP, 0.05 wt%, was added to the bassanite-containing paste, see Figure 1, it exhibited a considerable diminishing in viscosity, and a similar rheological behavior to those prepared with gypsum or anhydrite. The addition of SP to a cement paste can influence the hydration kinetics and hence, change the phase assemblage with time. However, the small amount of SP used in the bassanite-paste has not modified the phase assemblage (RQPA), in agreement with previous studies (García-Maté et al., 2015; García-Maté et al., 2012; Ma et al., 2014).

3.2. Hydrating reactions from the thermogravimetric analysis

Figure 2 depict the TG traces and the differential TG curves for gypsum and anhydrite pastes at different curing ages for the samples where the hydration was stopped as reported in the experimental section. Firstly, it should be highlighted that G10B2 at late ages has a larger degree of reaction with an overall weight loss of ~32 wt% at 365 hydration days which is larger than the corresponding value for G10B0, ~26 wt%. Using acetone for stopping the hydration did not affect the weight loss values of cement pastes. Table 1 gives the TGA loss (wt%) above 600ºC of different cement pastes at different hydration time. These low

values show lower influence of acetone in the hydration behavior. Moreover, total free water is large (for the same hydration ages) for G10B0 than for G10B2. Secondly, and very importantly, AFt which is characterized by the weight loss at ~100ºC slightly increases with hydrating time for G10B2, see Figure 2b, but it decreases with time for G10B0, see Figure 2a. The same behavior has been observed for A10B2 and A10B0, see Figures 2c and 2d. Table 1 gives specific surface areas of the cements determined by BET methodology. It is known that higher BET areas would yield to larger amounts of adsorbed acetone that will be lost from ~500ºC (Zhang and Scherer, 2011). However, this effect has not taken place in these experimental conditions as A10B0 cement presents a higher specific surface area than A10B2 and the weight loss is lower in the former at all ages, Figures 2c and 2d. In addition to the main weight loss measured at 100ºC, assigned to AFt, a second weight loss centered at ~180ºC, is attributed to stratlingite (Winnefeld and Lothenbach, 2010; Winnefeld and Barlag, 2010; Pelletier et al., 2010; Pelletier-Chaignat et al., 2011). Stratlingite formation is much faster in G10B0 pastes, being observed already at 3 days of hydration, than in G10B2 pastes. For G10B2, stratlingite formation is delayed and its content is smaller. All these crystalline phases can be quantified by powder diffraction and the results (see next section) are fully consistent with those reported here. Free water (FW) was determined by the difference between the added water and the combined water determined by thermogravimetric analysis (Álvarez-Pinazo et al., 2013) and the values are reported in Tables 2-7.

Table 1. TGA loss (wt%), from 600ºC to 1000ºC, for all studied cement pastes at different hydration time and specific surface area of all studied cements determined by BET methodology. Total sulfur content determined with XRF.

Hydration age (days)	G10B0	G10B2	A10B0	A10B2	B10B0	B10B2
3	0.62	0.77	0.83	0.67	0.76	0.75
7	0.70	0.73	0.89	0.69	0.64	0.83
28	0.96	0.77	0.97	0.77	1.15	0.92
120	1.21	0.87	0.87	1.09	1.50	1.23
180	0.90	1.15	1.66	0.98	-	-
365	1.67	1.56	1.64	1.21	-	-
BET area (m^2/g)	*1.13*	*1.81*	*1.35*	*1.12*	*1.36*	*1.61*
SO_3/wt%	*7.6*	*7.6*		*8.8*		*8.4*

Furthermore, thermal analysis is suitable to identify poor crystalline phases that cannot be analyzed by LXRPD, such as amorphous-AH3 (bound water around 250–300ºC), or even AFm (Winnefeld and Barlag, 2010; Telesca et al., 2014; Song et al., 2015). Since the AFm decomposition shows different peaks, and some are overlapped with other phases, it is difficult to be quantified; however, Figure 2a shows how AFm appears in G10B0 paste just after 3 days of hydration. Amorphous-AH_3 is detected in G10B2 pastes at 3 and 7, however, after 28 days, this signal disappears and the peak related to stratlingite develops, thus confirming that stratlingite is formed by consuming amorphous-AH_3. Similar conclusions can be drawn from the curves of A10B0 and A10B2, Figures 2c and 2d. On the other hand, amorphous-AH_3 signal is almost not evident in G10B0 traces, at any age. This is explained as it rapidly reacts to yield stratlingite which shows a strong signal at ages later than 3 days of hydration.

Table 2.- Rietveld quantitative phase analysis results for *G*10B0 cement paste, as a function of hydration time, including ACn calculated with G-method and free water content.

	t_0	3d	7d	28d	120d	180d	365d
β-C_2S	17.5(3)	17.0(3)	15.7(3)	8.9(4)	5.2(3)	4.2(3)	4.0(4)
o-$C_4A_3\bar{S}$	9.5(7)	2.2(1)	0.8(1)				
C_4AF	5.3(2)	4.1(2)	3.2(2)	1.1(2)			
C_2AS	3.7(2)	4.6(1)	4.3(1)	3.3(1)	3.3(1)	3.7(1)	3.4(1)
γ-C_2S	1.9(1)	1.8(1)	1.9(1)	1.5(1)	1.8(1)	1.7(1)	1.7(1)
CT	0.5(1)	0.4(1)	0.4(1)	0.2(1)	0.2(1)	0.2(1)	
$C\bar{S}H_2$	9.9(1)						
AFt		17.7(2)	15.9(2)	9.3(2)	9.6(3)	9.8(3)	10.6(3)
Stratlingite		4.1(6)	6.6(4)	12.5(2)	13.4(5)	10.6(5)	12.2(5)
AFm*			2.3(1)	5.5(2)	8.8(2)	10.8(2)	9.6(2)
Katoite&				2.3(4)	4.9(3)	4.6(2)	6.2(3)
CAH_{10}		0.4(1)	0.6(1)				
Hemicarbo					0.7(1)	1.0(1)	1.0(1)
$C\bar{C}$#							0.8(1)
ACn@	*16.1(8)*	*28.8(8)*	*30.7(6)*	*41.9(7)*	*37.5(8)*	*40.6(7)*	40.3(8)
FW$	35.5(1)	18.9(1)	17.6(1)	13.5(1)	14.7(-)	12.9(-)	10.2(-)

**Monosulfoaluminate; &siliceous hydrogarnet; #Calcite; @Amorphous and Crystalline non-quantified; $Free water.*

Table 3.- Rietveld quantitative phase analysis results for *G*10B2 cement paste, as a function of hydration time,

including ACn calculated with G-method and free water content. (Notation as in Table 2)

	t_0	3d	7d	28d	120d	180d	365d
α'_H-C_2S	18.6(4)	20.5(4)	20.0(4)	13.6(5)	5.0(6)	4.3(4)	4.4(6)
β-C_2S	1.1(2)	1.2(3)	1.3(2)	1.5(2)	2.1(2)	2.0(2)	2.3(2)
c-$C_4A_3\bar{S}$	10.5(1)	0.7(1)	0.2(1)				
C_4AF	5.1(2)	4.5(2)	4.4(2)	3.4(2)	1.1(2)	0.9(2)	0.9(2)
C_2AS	1.6(1)	2.5(1)	2.2(1)	2.1(1)	1.8(1)	1.8(1)	2.1(1)
CT	0.5(1)	0.7(1)	0.7(1)	0.5(1)			
$C\bar{S}H_2$	6.5(1)						
AFt		21.3(2)	21.8(2)	18.7(2)	19.1(2)	20.6(2)	20.8(2)
Stratlingite				10.2(4)	16.9(4)	17.4(4)	15.3(4)
AFm			0.2(1)	0.5(1)	1.8(1)	1.5(1)	1.0(1)
Katoite				0.5(1)	3.2(3)	3.9(3)	4.7(3)
AH_3		0.4(1)	0.5(1)				
ACn	*20.6(5)*	*30.7(6)*	*30.7(6)*	*35.8(7)*	*41.1(9)*	*44.9(7)*	*45.1(9)*
FW	*35.5(1)*	*17.5(1)*	*17.8(1)*	*13.1(1)*	*7.8(1)*	*2.6(1)*	*3.3(1)*

Table 4- Rietveld quantitative phase analysis results for *A*10B0 cement paste, as a function of hydration time, including ACn calculated with G-method and free water content. (Notation as in Table 2)

	t_0	3d	7d	28d	120d	180d	365d
β-C_2S	17.3(3)	17.1(3)	13.3(3)	10.9(4)	5.9(4)	5.9(5)	5.4(5)
o-$C_4A_3\bar{S}$	10.2(6)						
C_4AF	5.4(2)	3.3(2)	1.4(2)	1.2(2)	0.9(2)	1.0(2)	0.8(2)
C_2AS	2.9(2)	5.0(1)	4.6(1)	4.3(1)	4.6(2)	4.7(2)	4.6(2)
γ-C_2S	1.8(1)	1.4(1)	1.2(1)	1.4(1)	1.4(1)	1.4(1)	1.4(1)
CT	0.3(1)	0.3(1)	0.3(1)	0.3(1)			
$C\bar{S}$	7.5(1)						
AFt		22.2(2)	16.5(2)	17.2(2)	14.5(2)	11.6(2)	13.6(3)
Stratlingite		6.0(7)	13.4(5)	12.6(5)	10.2(6)	12.8(7)	11.5(7)
AFm			2.9(1)	2.4(1)	5.2(1)	4.6(1)	5.3(1)
Katoite			0.9(1)	2.1(2)	3.0(2)	3.2(2)	3.2(2)
CAH_{10}		0.3(1)					
Hemicarbo				0.5(1)	0.4(1)	0.6(1)	0.4(1)
$C\bar{C}$							1.5(1)
ACn	*19.1(7)*	*30.5(8)*	*33.9(7)*	*37.9(8)*	*43.5(8)*	*44.3(9)*	*46.2(1.0)*
FW	*35.5(1)*	*14.1(1)*	*11.6(1)*	*9.4(1)*	*10.5(1)*	*9.8(1)*	*6.2(1)*

Table 5.- Rietveld quantitative phase analysis results for *A*10B2 cement paste, as a function of hydration time, including ACn calculated with G-method and free water content. (Notation as in Table 2)

	t_0	3d	7d	28d	120d	180d	365d
α'_H- C_2S	19.2(4)	20.5(5)	17.1(5)	15.8(4)	6.6(6)	5.2(6)	5.9(6)
β-C_2S	0.8(1)	1.1(2)	0.9(3)	1.2(3)	2.3(5)	2.2(5)	2.4(5)
c-$C_4A_3\bar{S}$	11.2(1)	0.1(1)	0.2(1)				
C_4AF	5.9(2)	4.4(2)	3.8(2)	3.5(2)	1.3(2)	1.0(2)	0.9(2)
CT	0.7(1)	0.6(1)	0.6(1)	0.7(1)			
C_2AS	1.6(1)	2.2(1)	2.1(1)	2.4(1)	2.0(1)	1.8(1)	1.6(1)
$C\bar{S}$	6.8(1)						
AFt		24.1(2)	19.8(2)	25.0(2)	23.1(2)	22.3(2)	23.3(2)
Stratlingite				8.5(3)	16.3(4)	17.1(3)	13.6(4)
AFm				0.5(1)	1.2(1)	3.0(2)	1.1(1)
Katoite					2.5(4)	2.9(5)	3.5(5)
AH_3		0.3(1)	0.2(1)				
ACn							0.7(1)
FW	*18.3(5)*	*32.3(6)*	*36.6(7)*	*27.5(7)*	*41.2(1.0)*	*39.5(1.0)*	*42.4(1.1)*

Table 6- Rietveld quantitative phase analysis results for *B*10B0 cement paste, as a function of hydration time, including ACn calculated with G-method and free water content. (Notation as in Table 2)

	t_0	3d	7d	28d	120d
β-C_2S	18.9(4)	14.1(3)	13.4(3)	10.2(3)	5.4(3)
o-$C_4A_3\bar{S}$	9.4(7)	2.2(1)	1.2(1)		
C_4AF	5.0(2)	3.8(2)	3.6(2)	1.4(2)	0.9(2)
C_2AS	4.8(2)	3.9(1)	3.5(1)	3.6(1)	3.3(1)
γ-C_2S	1.4(1)	1.7(1)	1.6(1)	2.0(1)	1.8(1)
CT	0.4(1)	0.3(1)	0.2(1)	0.2(1)	0.2(1)

$C\bar{S}H_{0.5}$	5.2(2)				
AFt		15.9(3)	14.9(3)	12.6(3)	13.3(3)
Stratlingite		3.6(6)	4.2(6)	15.4(5)	12.1(5)
AFm		0.8(1)	1.0(1)	4.8(1)	5.4(2)
Katoite				3.3(4)	5.1(3)
Hemicarbo				0.5(1)	
ACn	*19.5(9)*	*32.5(8)*	*37.3(8)*	*31.3(8)*	*39.8(8)*
FW	*35.5(1)*	*21.3(1)*	*19.1(1)*	*14.6(1)*	*12.8(1)*

Table 7- Rietveld quantitative phase analysis results for *B*10B2 cement paste, as a function of hydration time, including ACn calculated with G-method and free water content. (Notation as in Table 2)

	t_0	3d	7d	28d	120d
α'_H- C_2S	20.8(4)	19.9(4)	20.6(5)	17.4(3)	4.0(5)
β-C_2S	0.4(1)	1.2(4)	1.1(3)	1.3(3)	2.1(3)
c-$C_4A_3\bar{S}$	11.9(1)	0.3(1)	0.3(1)		
C_4AF	5.2(2)	4.2(2)	4.0(2)	3.5(2)	0.6(2)
C_2AS	2.2(1)	2.3(1)	2.1(1)	2.6(1)	1.9(1)
CT	0.7(1)	0.7(1)	0.7(1)	0.7(1)	
$C\bar{S}H_{0.5}$	4.1(1)				
Aft		20.7(2)	19.7(2)	23.3(2)	19.5(2)
Stratlingite				5.0(6)	9.6(6)
AFm					1.1(2)
Katoite				0.9(2)	4.6(3)
AH_3		0.4(1)	0.5(1)	0.4(1)	0.4(1)
ACn	*19.3(5)*	*34.9(7)*	*36.2(7)*	*30.4(8)*	*47.7(9)*
FW	*35.5(1)*	*15.5(1)*	*14.9(1)*	*14.6(1)*	*8.6(1)*

3.3. Hydrating phase and chemical evolution from powder diffraction and electron microscopy

The phase evolutions with hydration have been followed by RQPA of the powder diffraction data and the chemical compositions of selected phases have been studied by electron microscopy. Tables 2-7 show the phase developments, including both ACn and free water (FW) contents, for both types of cement (active and non-active) prepared with 10 wt% of gypsum, anhydrite or bassanite. Figure 3 depicts AFt evolution with time for all the studied cements. Figure 4 shows LXRPD Rietveld patterns for A10B2 cement paste at 3 and 365 days of hydration, as representative examples; the main peaks are labeled to easily follow the phase evolution. The sulfate source was consumed before the first 3 days of hydration to form with time, ettringite as the main crystalline hydrated phase. AFm and stratlingite were also measured for all the studied pastes (Allevi et al., 2016) but in variable amounts.

As discussed previously from the thermal data study, there are important differences between active and non-active cements during hydration. After 3 days of hydration all the studied cement pastes yielded ettringite as main crystalline hydration product. However, this ettringite seems to be more stable in active cements (X10B2), which contained α'_H-C_2S and pseudo-cubic ye'elimite (see Tables 2-7), as it is almost constant with time of hydration, Figure 3. On the other hand, AFt contents decrease with time for X10B0 to give AFm phases. This could imply a decrease in the volume of hydrated products since AFm has lower volume than AFt. Consequently at later ages the amount of AFt is much larger in X10B2 and this is very likely the responsible of the improved mechanical properties of this family when compared to the poorer data for X10B0, Figure 3.

Now, we focus on belite reactivity. β-C_2S (present in X10B0) dissolves faster than α'_H-C_2S (present in X10B2) within the first 28 days, independently of the sulfate source, as can be seen in all the tables. Consequently, these cement pastes are silicon richer systems than X10B2 ones, and this may influence the previous discussed stability of AFt (Pelletier et al., 2010). In addition, crystalline stratlingite is quantified in X10B0 just after 3 days of hydration, but it is not detected until 28 days in X10B2 pastes, and C_4AF reacts quicker in G10B0 than in G10B2 (Tables 2 and 3, respectively), and it is completely dissolved in the former. However, at curing ages >28 days X10B0 family consumes some additional amounts of free water (FW), although the contents of anhydrous phases are almost kept constant. Finally, katoite (in this system is siliceous hydrogarnet, which may contain iron) is formed in both families but we cannot measure clear differences in behavior between the two families.

To finish the section devoted to the phase evolution from RQPA, the analysis of the data reported in Tables 2-7 indicate that the phase assemblage a latter ages are little sensitive to the initial sulfate source. AFt, stratlingite, katoite (siliceous hydrogarnet) and AFm contents between 120 and 365 days are very similar for G10B2 and A10B2. When comparing the results for G10B0 and A10B0, some (minor) differences are detected, for instance larger amounts of AFm in G10B0 than in A10B0.

The hydration of cement pastes is a process of ions dissolution, ions saturation, and then precipitation of new phases. An EDX-SEM study was performed to better characterize the chemical

composition of each phase in the hydrated X10B2 pastes, especially for amorphous/ill-crystalline phases. X10B2 pastes were selected since the obtained RQPA data for these pastes indicate higher ettringite contents than for X10B0; hence active-mortars are expected to show higher mechanical strengths than the non-active ones under same conditions (Álvarez-Pinazo et al., 2013). This type of study is essential to understand how and where Si, Al and Fe ions, once they are in solution, will form new crystalline or amorphous phases with time, since this may affect the mechanical properties (Taylor, 1997). Figure 5 shows Fe/Ca vs. Si/Ca atomic ratios for the three X10B2 cement pastes at 120 days of hydration. Theoretical chemical compositions of some phases have been included as solid symbols for the sake of comparison. Representative micrographs are also shown in Figure 5. Amorphous phases have been identified in the micrographs as particles, or group of particles, without a defined shape and their chemical compositions are far from all the theoretical compositions included in the figure. SEM-EDX analyses of these hydrated pastes reveal that the chemical composition of amorphous phase(s) in G10B2 and B10B2 are very similar, but slightly richer in silicon and iron in A10B2.

The chemical composition evolution with time is quite interesting to understand as it could allow having a better insight of the effects of the belite polymorphism and the sulfate source during hydration. Figures 6a and 6b show Al-Si atomic ratio, for A10B2 paste at 7 and 120 days of hydration, respectively; representative micrographs of the pastes are also provided in the figure. These results reveal that particles without a defined shape, which may be amorphous phases, are rich in aluminum at early ages (7 days), while they are enriched in silicon with time (120 days). The former is related to reactions 1 and 2, and the latter with the reactivity of belite (Eq. 4). As stated above, C_4AF phase is reacting at early ages, however, hydration products which contain iron are difficult to be identified by LXRPD. Figure 7 shows Al-Fe atomic ratio for A10B2 pastes at the same ages (7 and 120 days). When analyzing particles with a needle shape, which are identified as ettringite, some amounts of iron are found. These results may indicate that iron is incorporating in AFt crystal structure, in agreement with previous reports (Möschner et al., 2009). However, the unit cell volumes of AFt in A10B2 at 7 and 120 days are 2350.4(1) and 2340.2(2) Å3, respectively. An iron containing AFt should present a higher unit cell volume than that of AFt obtained from ye'elimite hydration (2346.9(4) Å3) (Cuesta et al., 2014). These unit cell volume values do not help to clarify if iron is being incorporated in AFt in these experimental conditions. Consequently, more research is needed. In addition, the sample hydrated for 7 days shows some small bright particles with a chemical composition similar to that of stratlingite; the DTA thermograph of this sample, Figure 2d, shows a small shoulder at ~170ºC, which is related to stratlingite. However, these particles seem to have low crystallinity degree, and so they cannot be detected by LXRPD at that hydration age. The iron content in these bright particles increase from ~0.05 Fe/Ca atomic ratio at 7 days to ~0.1 Fe/Ca atomic ratio at 120 days. These results may be interpreted assuming two possibilities, although we are aware that more research is needed: i) there is an iron-bearing hydrated amorphous phase on the surface of stratlingite particles; or ii) the reaction between belite and ferrite gives an iron-bearing stratlingite by Eq. 6, rather than Eq. 3 given in the introduction section:

$$C_2S + x\ C_4AF + (1\text{-}2x)\ AH_3 + (10x+5)\ H \rightarrow C_2A_{1-x}F_xSH_8 + 4x\ CH \quad (6)$$

3.4. Compressive strengths of BYF mortars

Figure 8 shows mechanical strengths of the mortars studied in this work with a constant w/c ratio of 0.55. We highlight that larger mechanical strengths can be attained with lower w/c ratios (0.35-0.40), but then to follow the chemical evolution is tougher as local drying effects may start to appear. More studies where variable w/c ratios and curing conditions are correlated with phase evolutions and strength developments are needed in order to understand the thorough hydrating behavior for this emerging type of cements.

First of all, mortars prepared with the non-active BYF cement, Figure 8a, developed lower compressive strengths than active mortars (Figure 8b), as previously reported (Álvarez-Pinazo et al., 2013; Li et al., 2007), independently of the sulfate source. Within the non-active mortars, A10B0 presented the highest values. This behavior may be explained/justified by the higher BET area value (Table 1) and the slightly higher stability of AFt present in A10B0 paste (Table 4) which lead to lower amounts of AFm, when compared to G10B0 (Table 2). The recrystallization of AFm from AFt may partly change the microstructure of the hardened pastes and consequently has a negative effect on mechanical strengths. In addition, since the setting time of A-pastes is longer than that for G-pastes, the former show higher plasticity that can better accommodate the precipitation of ettringite (García-Maté et el., 2015). Bassanite cement reacts very quickly with water showing a short setting time which lead to mortars with low degree of homogeneity, as discussed above. Due to this behavior, the compressive strength values for B10B0 mortars were not measured. For B10B2, although the addition of a small amount of SP improved the workability of the mortar at very early ages, the delay in the setting time was not enough to develop comparable mechanical strength values to gypsum and anhydrite mortars at early hydration time, see Figure 8b. This may be also due to the lower hydration degree induced by the use of SP.

G10B2 and A10B2 mortars present very similar compressive strengths values up to 7 days (figure 8), and their pastes also show similar ettringite contents. However, at 28 hydration days,

A10B2 mortar shows slightly higher strength value, which again can be justified by a larger amount of ettringite (25 and 19 wt% for A and G-pastes, respectively). However, at 120 days G10B2 mortar developed the highest mechanical strength value, even when the amount of ettringite for the A-paste is slightly larger than that for G-paste (23 and 19 wt%, respectively) and the chemical composition of amorphous phases are richer in silicon (SEM-EDX analyses, Figure 5). Therefore, we are forced to conclude that the amorphous contents are playing a key role for the strength development at late ages. Moreover, G10B2 cement has the highest BET value (Table 1) of all the studied cements and this may also justify this behavior. The reaction degree of α'_H-C_2S in G10B2 (74%) is slightly higher than that in A10B2 (65%), which could help in improving the mechanical strengths. The strength increases by increasing the amount of hydrates being formed and a declining amount of non-hydrated material (Odler, 2003).

4. Conclusions

The effect of the sulfate source (G-gypsum, A-anhydrite and B-bassanite) and the polymorph phase (belite and ye'elimite) of two laboratory-prepared BYF cements was studied during hydration. The obtained results were correlated with the compressive strengths of the corresponding mortars. Non-active cements (X10B0) that contain orthorhombic ye'elimite (and β-C_2S) showed larger amounts of AFm and consequently, lower quantities of ettringite during hydration when compared to active cements (X10B2) which contain pseudo-cubic ye'elimite (and α'_H-C_2S). For X10B0 mortars, those prepared with anhydrite presented the highest compressive strength values (f.i. 32±1 MPa at 120 days). The chemical compositions of amorphous phases in active-pastes, at 120 days of hydration, prepared with gypsum or bassanite (G10B2 and B10B2) were very similar, but slightly richer in silicon when anhydrite (A10B2) was used. In addition, for the latter, amorphous phases, at 7 days of hydration, were richer in aluminum than those after 120 days. Moreover, this sample (A10B2) shows ettringite particles that contain iron, at 7 and 120 hydration days. Active-mortars prepared with gypsum or anhydrite showed very similar compressive strengths values up to 7 days (25±1 MPa at 7 days), since their pastes show similar ettringite contents. However, at 120 days, the G10B2 mortar developed the highest mechanical strength value (68±1 MPa), even when its amount of ettringite was slightly lower than that for the A-samples.

Figure Captions

Figure 1. Flow curves of G10B2, A10B2, B10B2 and B10B2 with 0.05 wt% superplasticizer pastes.

Figure 2. Thermogravimetric analyses for: (a) G10B0, (b) G10B2, (c) A10B0 and (d) A10B2 pastes after stopping hydration at 3, 7, 28, 120, 180 and 365 days.

Figure 3. Amount of AFt determined by Rietveld method with time for all the studied cements.

Figure 4. Rietveld LXRPD patterns of A10B2 hydrated at (a) 3 days and (b) 365 days. Main peaks due to a given phase have been labeled. $C\bar{C}$, AFt, Strat, Kat and AFm, stands for calcite, ettringite, stratlingite, siliceous hydrogarnet and monosulfoaluminate, respectively.

Figure 5. Fe/Ca atomic ratio vs. Si/Ca atomic ratio for EDX-SEM study of the X10B2 pastes at 120 days. Solid symbols represent the theoretical composition of the phases. Notation as in Figure 4.

Figure 6. Al/Ca atomic ratio vs. Si/Ca atomic ratio for EDX-SEM study of the A10B2 pastes at (a) 7 days, and (b) 120 days. Solid symbols represent the theoretical composition of the phases. Notation as in Figure 4. C-S-H stands for calcium silicate gel with average composition Si/Ca=0.59 (Scrivener et al., 2004)

Figure 7. Al/Ca atomic ratio vs. Fe/Ca atomic ratio for EDX-SEM study of the A10B2 pastes at (a) 7 days and (b) 120 days. Solid symbols represent the theoretical composition of the phases. Notation as in Figure 4.

Figure 8. Compressive strength values of mortars prepared from all pastes at different hydration times (3, 7, 28 and 120 days).

Acknowledgments

This work is part of the PhD work of G. Álvarez-Pinazo funded by MINECO BES-2011-044690 grant. Funding from Junta de Andalucía (P11-FQM-7517), Spanish MINECO (BIA2014-57658-C2-2-R, which is co-funded by FEDER, and BIA2014-57658-C2-1-R research grants.

References

*Álvarez-Pinazo G, Cuesta A, García-Maté M et al. (2012) Rietveld quantitative phase analysis of yeelimite-containing cements. Cement and Concrete Research **42(7)**:960-971.*

*Álvarez-Pinazo G, Cuesta A, García-Maté M et al. (2014) In-situ early-age hydration study of sulfobelite cements by synchrotron powder diffraction. Cement and Concrete Research **56(1)**:12–19.*

*Álvarez-Pinazo G, Santacruz I, León-Reina L et al. (2013) Hydration reactions and mechanical strength developments of iron-rich sulfobelite eco-cements. Industrial & Engineering Chemistry Research **52(47)**:16606−1661.*

*Allevi S, Marchi M, Scotti F et al. (2016) Hydration of calcium sulphoaluminate clinker with additions of different calcium sulphate sources. Materials and Structures **49(1):** 453-466.*

Aranda MAG and De la Torre AG (2013) Sulfoaluminate cement (Pacheco-Torgal F, Jalali S, Labrincha J, John VM (Eds.)) Eco-efficient concrete, Woodhead Publishing Limited. Cambridge, pp. 488-522.

Aranda MAG, De la Torre AG and León-Reina L (2012) Rietveld quantitative phase analysis of OPC clinkers, cements and hydration products. Reviews in Mineralogy and Geochemistry ***74****:169-209.*

Benarchid MY, Diouri A, Boukhari A et al. (2004) Elaboration and thermal study of iron-phosphorus-substituted dicalcium silicate phase. Cement and Concrete Research ***34(10)****:1873–1879.*

Bensted J (1979) Some hydration studies of α-dicalcium silicate. Cement and Concrete Research ***9(1)****:97–101.*

Berger S, Cau-Dit-Coumes C, Le Bescop P et al. (2011) Influence of a thermal cycle at early age on the hydration of calcium sulphoaluminate cements with variable gypsum contents. Cement and Concrete Research ***41(2)****:149–160.*

Chatterjee AK (1996) High belite cements present status and future technological options: Part I and Part II. Cement and Concrete Research ***26****:1213−1237.*

Chen IA, Hargis CW and Juenger MCG (2012) Understanding expansion in calcium sulfoaluminate–belite cements. Cement and Concrete Research ***42(1)****:51–60.*

Cline JP, Von Dreele RB, Winburn R et al. (2011) Addressing the amorphous content issue in quantitative phase analysis: the certification of NIST standard reference material 676a. Acta Crystallographica Section A ***67(4):*** *357-367.*

Cuberos AJM, De la Torre AG, Alvarez-Pinazo G et al (2010) Active iron-rich belite sulfoaluminate cements: clinkering and hydration. Environmental Science & Technology ***44(17)****:6855-6862.*

Cuesta A, Álvarez-Pinazo G, Sanfélix SG et al. (2014) Hydration mechanisms of two polymorphs of synthetic ye'elimite. Cement and Concrete Research ***63****:127–136.*

De la Torre AG, Cabeza A, Calvente A et al. (2001) Full Phase Analysis of Portland Clinker by Penetrating Synchrotron Powder Diffraction. Analytical Chemistry ***73(2)****:151−156.*

Dilnesa BZ, Lothenbach B, Renaudin G et al. (2012) Stability of monosulfate in the presence of iron. Journal of the American Ceramic Society ***95(10)****:3305−3316.*

Dollase WA (1986) Correction of intensities for preferred orientation in powder diffractometry: application of the March model. Journal of Applied Crystallography ***19(4)****: 267-272.*

Fierens P and Tirlocq J (1983) Nature and concentration effect of stabilizing elements of Beta-dicalcium silicate on its hydration rate. Cement and Concrete Research ***13(2)****:267–276.*

Finger LW, Cox DE and Jephcoat AP (1994) A correction for powder diffraction peak asymmetry due to diaxial divergence. Journal of Applied Crystallography ***27(6):*** *892-900.*

Flatt RJ, Roussel N and Cheeseman CR (2012) Concrete: an eco material that needs to be improved. Journal of the European Ceramic Society ***32(11)****: 2787–2798.*

Fukuda K, Takeda A and Yoshida H (2001) Remelting reaction of α*-*Ca_2SiO_4 *solid solution confirmed in* Ca_2SiO_4*–*$Ca_{12}Al_{14}O_{33}$ *pseudobinary system. Cement and Concrete Research* ***31(8)****:1185–1189.*

García-Maté M, De la Torre AG, León-Reina L et al. (2013) Hydration studies of calcium sulfoaluminate cements blended with fly ash. Cement and Concrete Research ***54****:12–20.*

García-Maté M, De la Torre AG, Leon-Reina L et al. (2015) Effect of calcium sulfate source on the hydration of calcium sulfoaluminate eco-cement. Cement and Concrete Composites ***55****:53–61.*

García-Maté M, Santacruz I, De la Torre AG et al. (2012) Rheological and hydration characterization of calcium sulfoaluminate cement pastes. Cement and Concrete Composites ***34(5)****:684–691.*

Gartner EM (2004) Industrially interesting approaches to "low - CO2" cements. Cement and Concrete Research ***34(9)****:1489-1498.*

Garnet E and Hirao H (2015) A review of alternative approaches to the reduction of CO2 emissions associated with the manufacture of the binder in concrete. Cement and Concrete Research ***78****:126–142.*

Gies A and Knofel D (1987) Influence of sulfur on the composition of belite-rich cement clinkers and the technological properties of the resulting cements. Cement and Concrete Research ***17(2)****:317−328.*

Hasanbeigi A, Menke C and Price L (2010) The CO_2 *abatement cost curve for the Thailand cement industry. Journal of Cleaner Production* ***18(15)****:1509–1518.*

Jansen D, Goetz-Neunhoeffer F, Stabler CH et al. (2011) A remastered external standard method applied to the quantification of early OPC hydration. Cement and Concrete Research ***41(6):*** *602-608.*

Kantro DL and Weise CH (1979) Hydration of various beta-dicalcium silicate preparations. Journal of the American Ceramic Society ***62(11-12)****:621–626.*

Larson AC and Von Dreele RB (2000) General Structure Analysis System (GSAS), Los Alamos National Laboratory Report LAUR, 86-748.

Li GS and Gartner EM (2006) High-belite sulfoaluminate clinker: fabrication process and binder preparation. World Patent Application WO 2006/018569 A2, 23 Feb 2006.

Li GS, Walenta G and Gartner EM (2007) Formation and hydration of low-CO_2 *cements based on belite, calcium sulfoaluminate and calcium aluminoferrite. Proceedings of the 12th ICCC. Montreal, Canada, TH3-15.3.*

Ma B, Ma M, Shen X et al. (2014) Compatibility between a polycarboxylate superplasticizer and the belite-rich sulfoaluminate cement: Setting time and the hydration properties. Construction and Building Materials ***51****:47–54.*

Martín-Sedeño MC, Cuberos AJM, De la Torre AG et al. (2010) Aluminium-rich belite sulfoaluminate cements: Clinkering and early age hydration. Cement and Concrete Research ***40(3)****:359−369.*

Matkovic B, Carin V, Gacesa T et al. (1981) Influence of $BaSO_4$ *on the formation and hydration properties of calcium silicates: I,*

Doped Dicalcuim Silicates. American Ceramic Society Bulletin ***60****:825–829.*

Möschner G, Lothenbach B, Winnefeld F et al. (2009) Solid solution between Al-ettringite and Fe-ettringite $(Ca_6[Al_{1-x}Fe_x(OH)_6]_2(SO_4)_3 \cdot 26H_2O)$*. Cement and Concrete Research* ***39(6)****:482−489.*

O'Connor BH and Raven MD (1998) Application of the Rietveld refinement procedure in assaying powdered mixtures. Powder Diffraction ***3****: 2-6.*

Odler I (2003) Hydration, Setting and Hardening of Portland Cement. In: Lea's Chemistry of Cement and Concrete, 4th Ed. Elsevier.

Odler I and Abdul-Maula S (1984) Possibilities of quantitative determination of the AFt-(ettringite) and AFm-(monosulphate) phases in hydrated cement pastes. Cement and Concrete Research ***14(1)****:133–141.*

Pelletier L, Winnefeld F and Lothenbach B (2010) The ternary system Portland cement–calcium sulphoaluminate clinker–anhydrite: hydration mechanism and mortar properties. Cement and Concrete Composites ***32(7)****:497–507.*

Pelletier-Chaignat L, Winnefeld F, Lothenbach B et al. (2011) Influence of the calcium sulphate source on the hydration mechanism of Portland cement–calcium sulphoaluminate clinker–calcium sulphate binders. Cement and Concrete Composites ***33(5)****:551–561.*

Pera J and Ambroise J (2004) New applications of calcium sulfoaluminate cement. Cement and Concrete Research ***34(4)****:671-676.*

Scrivener KL, Fullmann T, Gallucci E et al. (2004) Quantitative study of Portland cement hydration by X-ray diffraction/Rietveld analysis and independent methods. Cement and Concrete Research ***34(9):****1541-1547.*

Song F, Yu Z, Yang F et al. (2015) Microstructure of amorphous aluminum hydroxide in belite-calcium sulfoaluminate cement. Cement and Concrete Research ***71(1)****:1–6.*

Taylor HFW (1997) Cement Chemistry, 2nd ed. Telford, UK.

Telesca A, Marroccoli M, Pace ML et al. (2014) A hydration study of various calcium sulfoaluminate cements. Cement and Concrete Composites ***53****:224–232.*

Thompson P, Cox DE and Hasting JB (1987) Rietveld refinement of Debye-Scherrer synchrotron X-ray data from Al_2O_3*. Journal of Applied Crystallography* ***20****: 79-83.*

Van Oss HG and Padovani AC (2003) Cement manufacture and the environment, Part II: environmental challenges and opportunities. Journal of Industrial Ecology ***7(1)****:93–126.*

Walenta G and Comparet C (2011) New Cements and Innovative Binder Technologies BYFF cements-recent developments. In: ECRA-Barcelona-2011. http://www.aether-cement.eu/press-room/publications/aethercement-ecra-barcelona-presentation-2011-05-05.html.

Wang J (2010) Hydration mechanism of cements based on low-CO2 clinkers containing belite, ye'elimite and calcium alumino-ferrite. PhD Thesis. Lille, University of Lille.

Winnefeld F and Barlag S (2010) Calorimetric and thermogravimetric study on the influence of calcium sulfate on the hydration of ye´elimite. Journal of Thermal Analysis and Calorimetry ***101(3)****:949–957.*

Winnefeld F and Lothenbach B (2010) Hydration of calcium sulfoaluminate cements - Experimental findings and thermodynamic modeling. Cement and Concrete Research ***40(8)****:1239-1247.*

Zhang J and Scherer GW (2011) Comparison of methods for arresting hydration of cement. Cement and Concrete Research ***41(10)****:1024–1036.*

Ziemer B, Altrichter B and Jesenak V (1984) Effect of SO_3 *on formation and hydraulic reactivity of belite. Cement and Concrete Research* ***14(5)****:686–692.*

“Hydration of Belite-Ye'elimite-Ferrite (BYF) cements with different calcium sulfate sources” ACR-D-16-00030.

List of table and figure captions.

Table 1. TGA loss (wt%), from 600ºC to 1000ºC, for all studied cement pastes at different hydration time and specific surface area of all studied cements determined by BET methodology. Total sulfur content determined with XRF.

Table 2.- Rietveld quantitative phase analysis results for G10B0 cement paste, as a function of hydration time, including ACn calculated with G-method and free water content.

Table 3.- Rietveld quantitative phase analysis results for G10B2 cement paste, as a function of hydration time, including ACn calculated with G-method and free water content. (Notation as in Table 2)

Table 4- Rietveld quantitative phase analysis results for A10B0 cement paste, as a function of hydration time, including ACn calculated with G-method and free water content. (Notation as in Table 2)

Table 5.- Rietveld quantitative phase analysis results for A10B2 cement paste, as a function of hydration time, including ACn calculated with G-method and free water content. (Notation as in Table 2)

Table 6- Rietveld quantitative phase analysis results for B10B0 cement paste, as a function of hydration time, including ACn calculated with G-method and free water content. (Notation as in Table 2)

Table 7- Rietveld quantitative phase analysis results for B10B2 cement paste, as a function of hydration time, including ACn calculated with G-method and free water content. (Notation as in Table 2)

Figure 1. Flow curves of G10B2, A10B2, B10B2 and B10B2 with 0.05 wt% superplasticizer pastes.

Figure 2. Thermogravimetric analyses for: (a) G10B0, (b) G10B2, (c) A10B0 and (d) A10B2 pastes after stopping hydration at 3, 7, 28, 120, 180 and 365 days.

Figure 3. Amount of AFt determined by Rietveld method with time for all the studied cements.

Figure 4. Rietveld LXRPD patterns of A10B2 hydrated at (a) 3 days and (b) 365 days. Main peaks due to a given phase have been labeled. $C\bar{C}$, AFt, Strat, Kat and AFm, stands for calcite, ettringite, stratlingite, siliceous hydrogarnet and monosulfoaluminate, respectively.

Figure 5. Fe/Ca atomic ratio vs. Si/Ca atomic ratio for EDX-SEM study of the X10B2 pastes at 120 days. Solid symbols represent the theoretical composition of the phases. Notation as in Figure 4.

Figure 6. Al/Ca atomic ratio vs. Si/Ca atomic ratio for EDX-SEM study of the A10B2 pastes at (a) 7 days, and (b) 120 days. Solid symbols represent the theoretical composition of the phases. Notation as in Figure 4. C-S-H stands for calcium silicate gel with average composition Si/Ca=0.59 (Scrivener et al., 2004)

Figure 7. Al/Ca atomic ratio vs. Fe/Ca atomic ratio for EDX-SEM study of the A10B2 pastes at (a) 7 days and (b) 120 days. Solid symbols represent the theoretical composition of the phases. Notation as in Figure 4.

Figure 8. Compressive strength values of mortars prepared from all pastes at different hydration times (3, 7, 28 and 120 days).

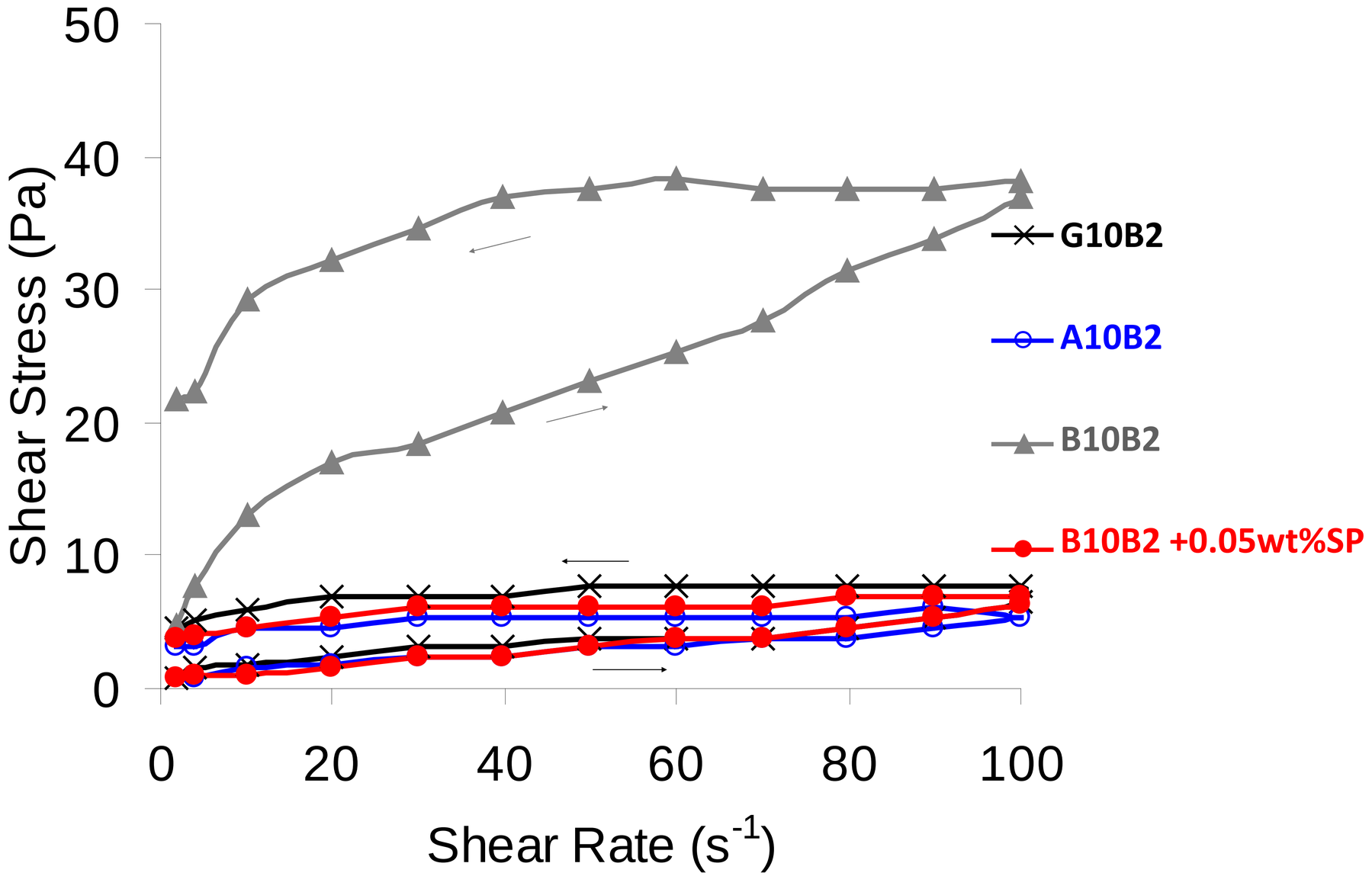
Shear Stress (Pa)
50
40
30
20
10
0
0
20
40
60
80
100
Shear Rate (s-1)
G10B2
A10B2
B10B2
B10B2 +0.05wt%SP

(a) *G*10B0

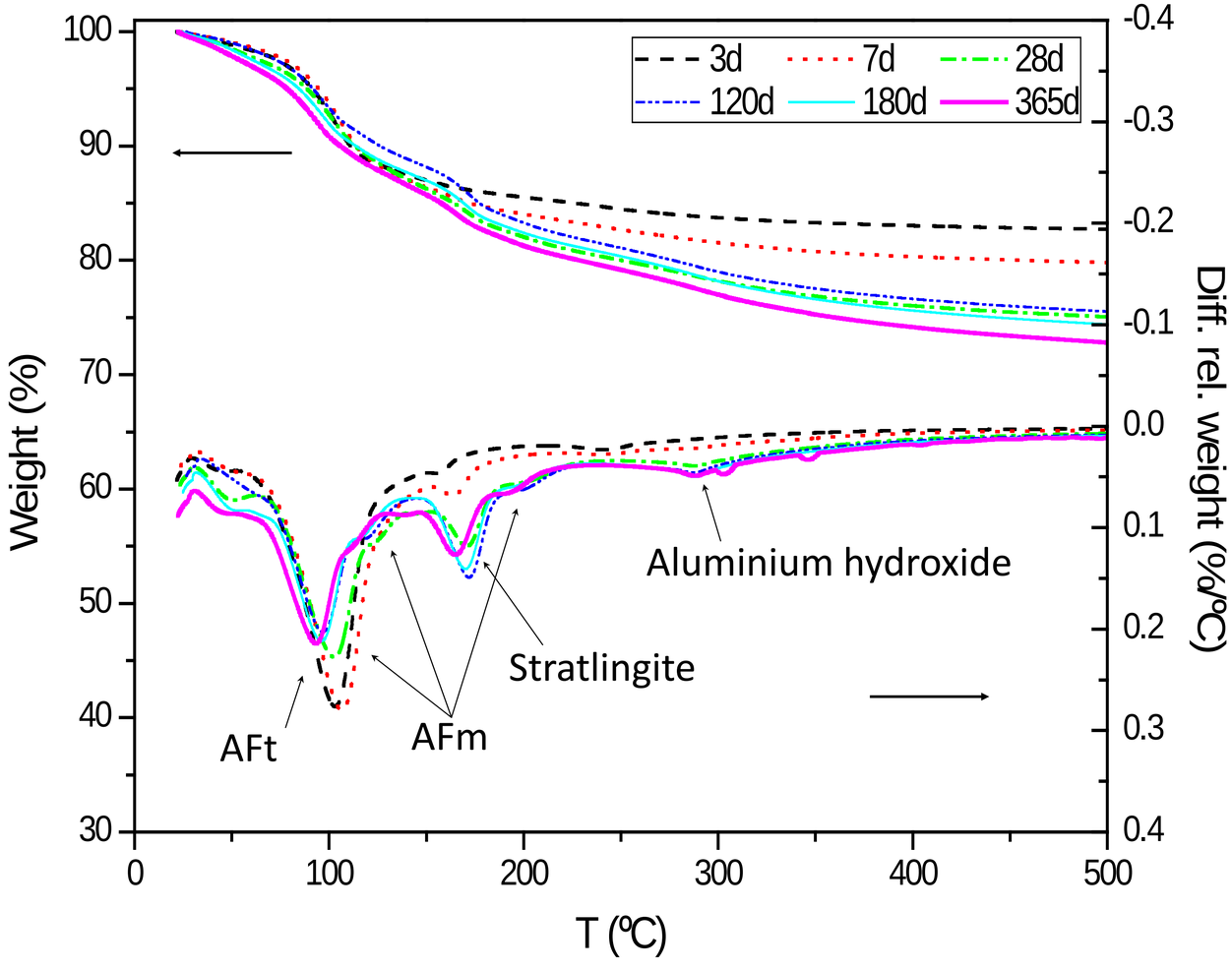

(b) *G*10B2

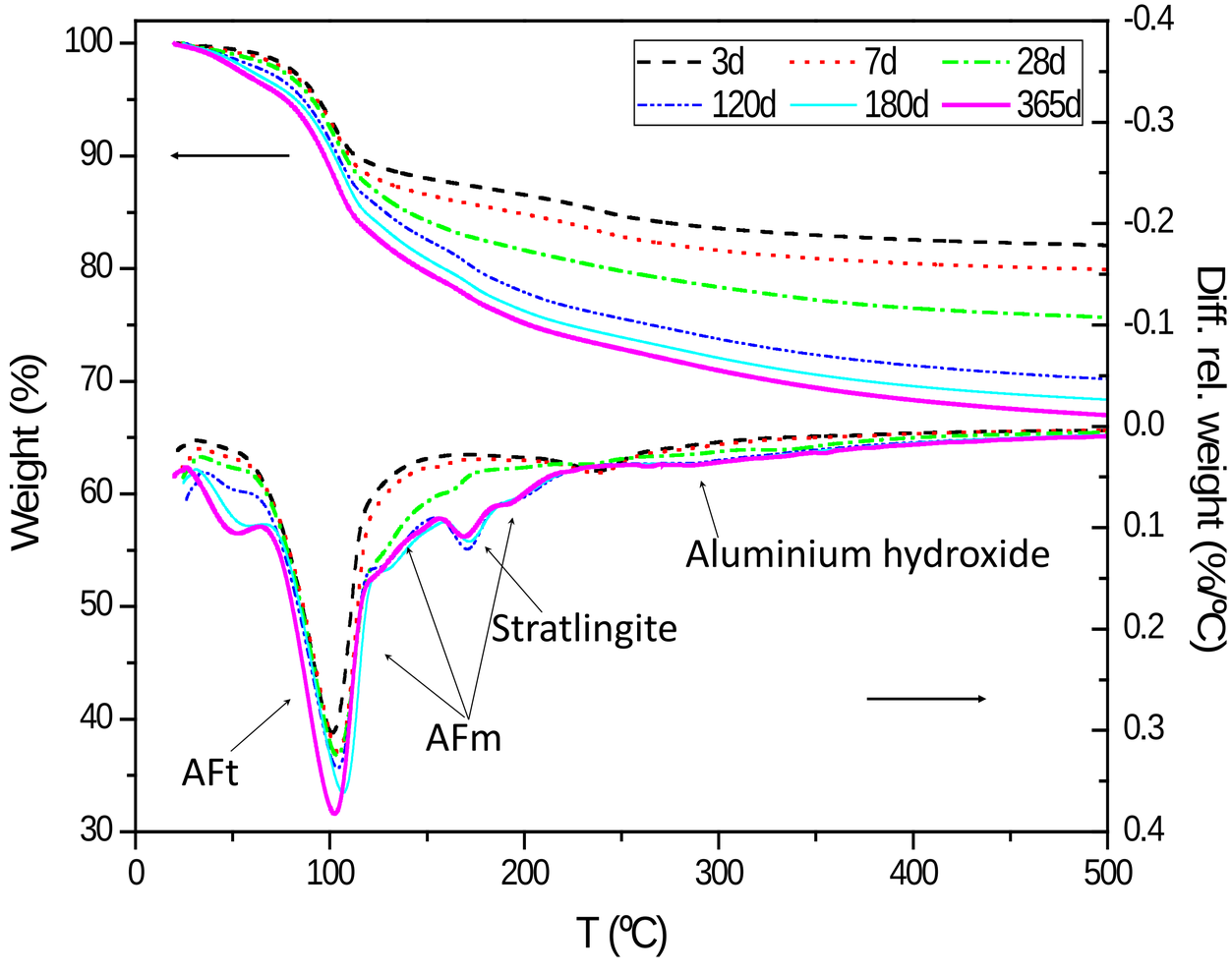

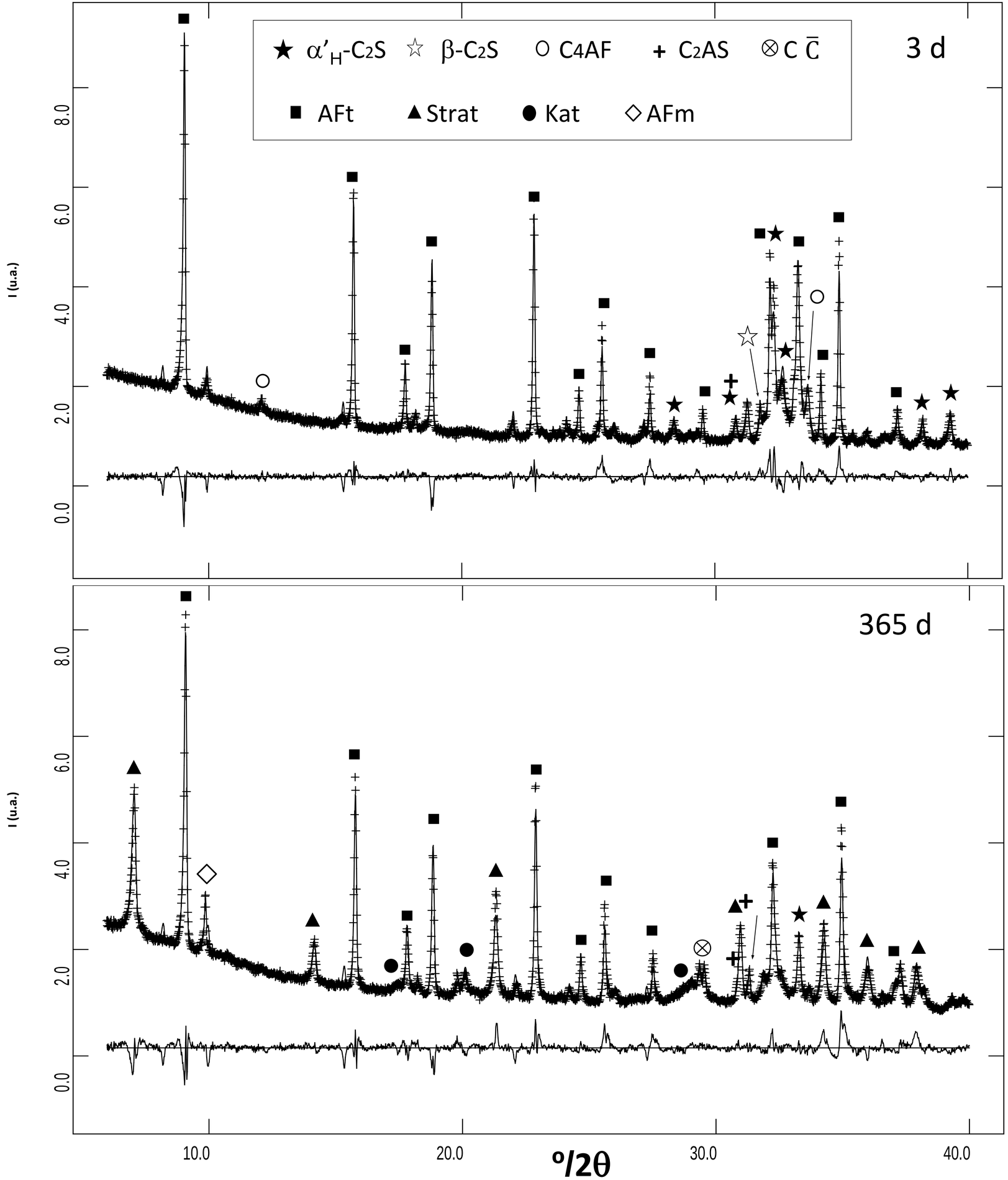
★ α'H-C2S
☆ β-C2S
○ C4AF
+ C2AS
⊗ C C̄
■ AFt
▲ Strat
● Kat
◇ AFm
3 d
365 d
I (u.a.)
0.0
2.0
4.0
6.0
8.0
10.0
20.0
30.0
40.0
º/2θ

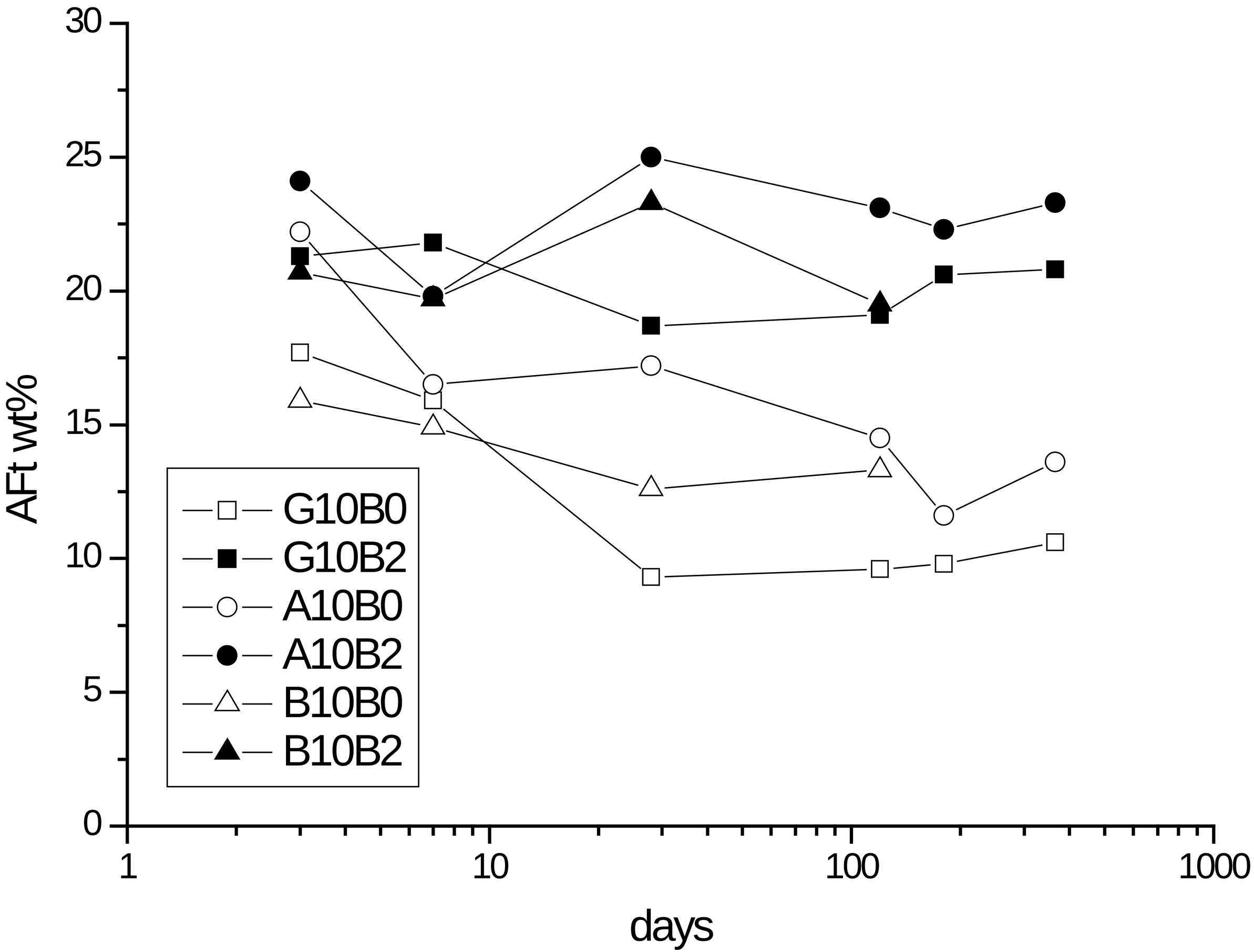
AFt wt%
30
25
20
15
10
5
0
1
10
100
1000
days
G10B0
G10B2
A10B0
A10B2
B10B0
B10B2

▲ C_2S/Strat ● C_4AF ▼Kat ★ AFt

○ *A*10B2 ✱ *B*10B2 △ *G*10B2

Fe/Ca atomic ratio

Si/Ca atomic ratio

0.0 0.1 0.2 0.3 0.4 0.5 0.6

0.0 0.1 0.2 0.3 0.4 0.5 0.6 0.7

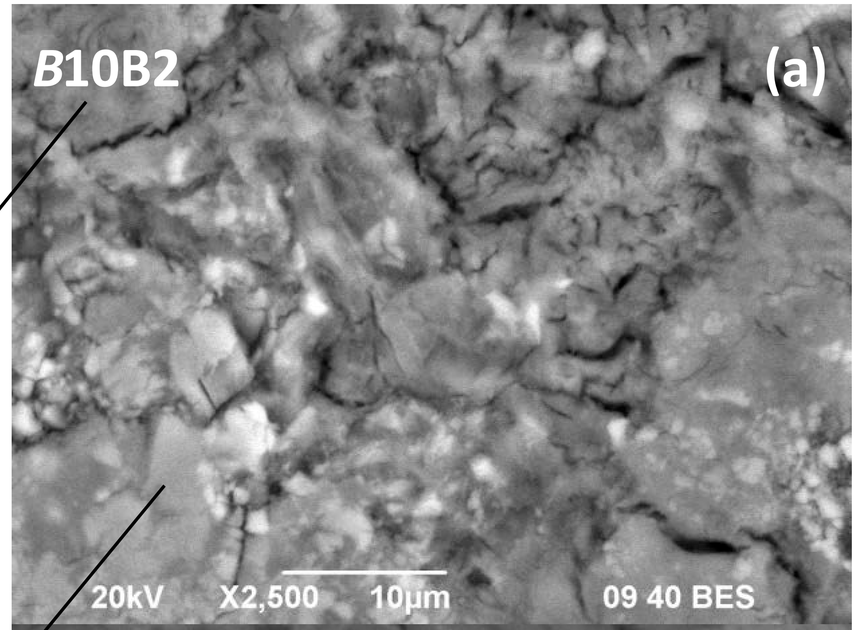

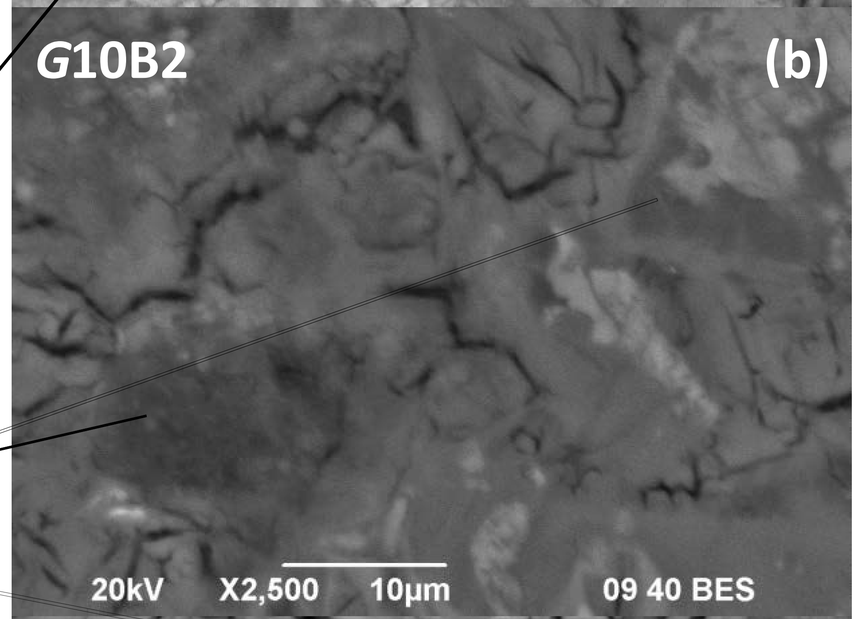

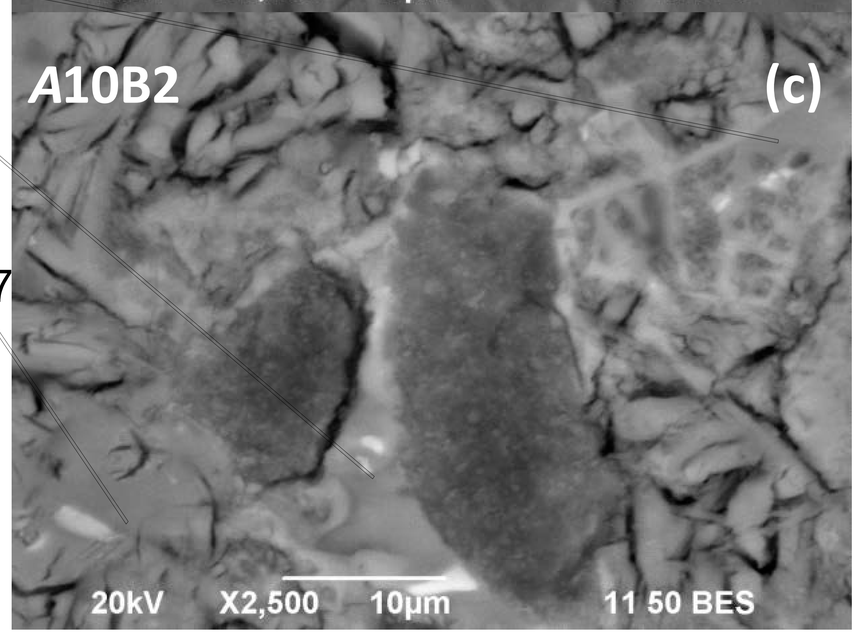

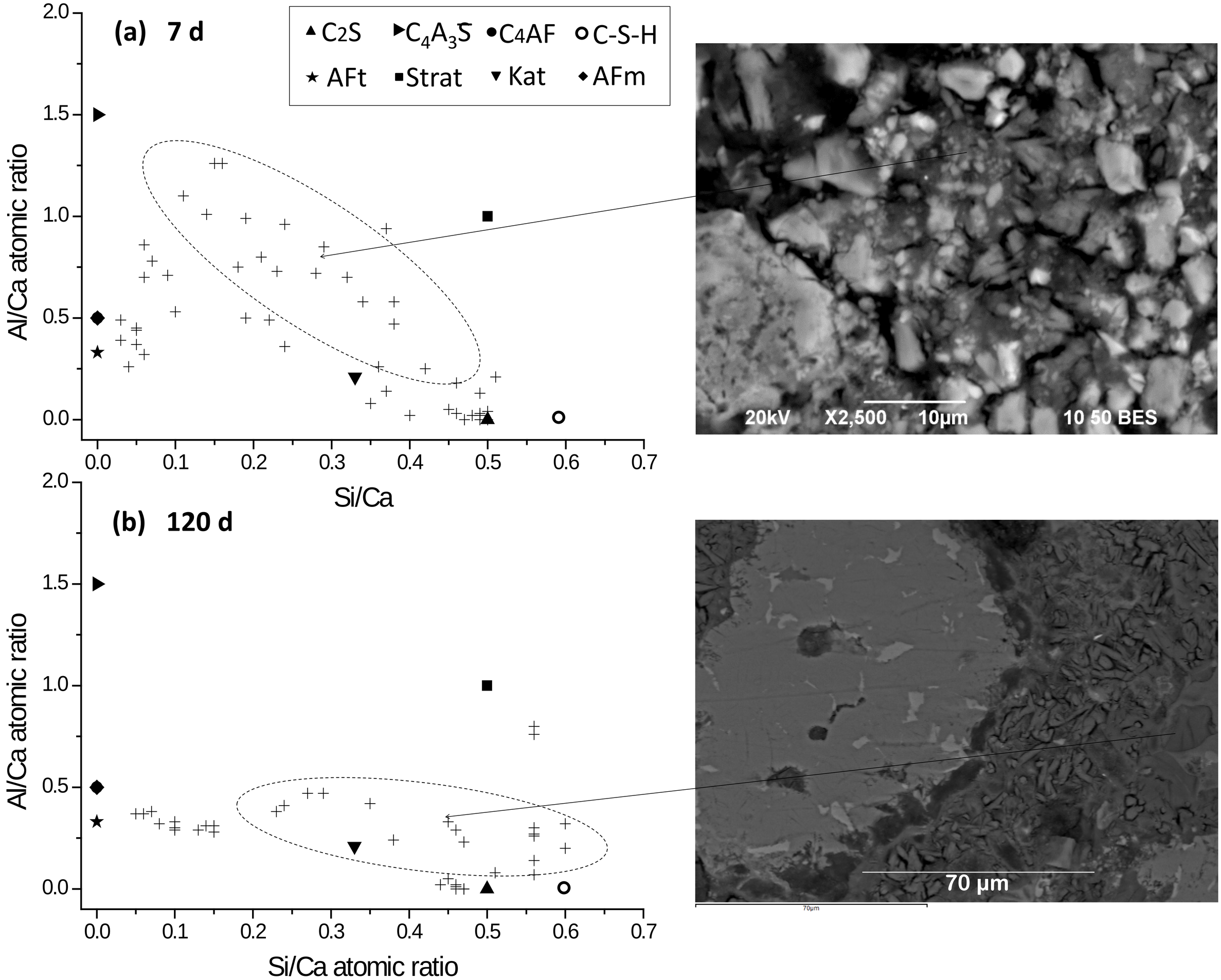
(a) 7 d
C2S
C4A3S
C4AF
C-S-H
AFt
Strat
Kat
AFm
Al/Ca atomic ratio
2.0
1.5
1.0
0.5
0.0
0.0
0.1
0.2
0.3
0.4
0.5
0.6
0.7
20kV X2,500 10μm 10 50 BES
(b) 120 d
Si/Ca
Al/Ca atomic ratio
Si/Ca atomic ratio
70 μm
70μm

(a) 7 d

▲ C_2S ▶ $C_4A_3\underline{S}$ ● C_4AF

★ AFt ■ Strat ▼ Kat ◆ AFm

Al/Ca

2.0
1.5
1.0
0.5
0.0

0.0 0.1 0.2 0.3 0.4 0.5 0.6

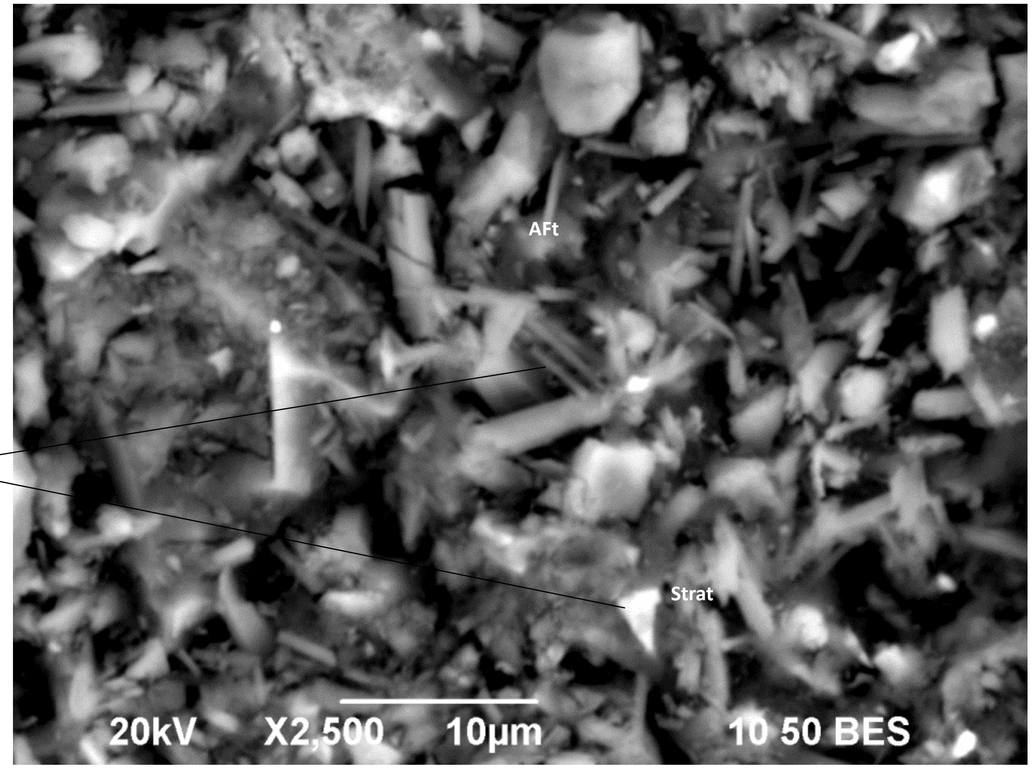

(b) 120 d

Fe/Ca

Al/Ca

2.0
1.5
1.0
0.5
0.0

0.0 0.1 0.2 0.3 0.4 0.5 0.6

Fe/Ca

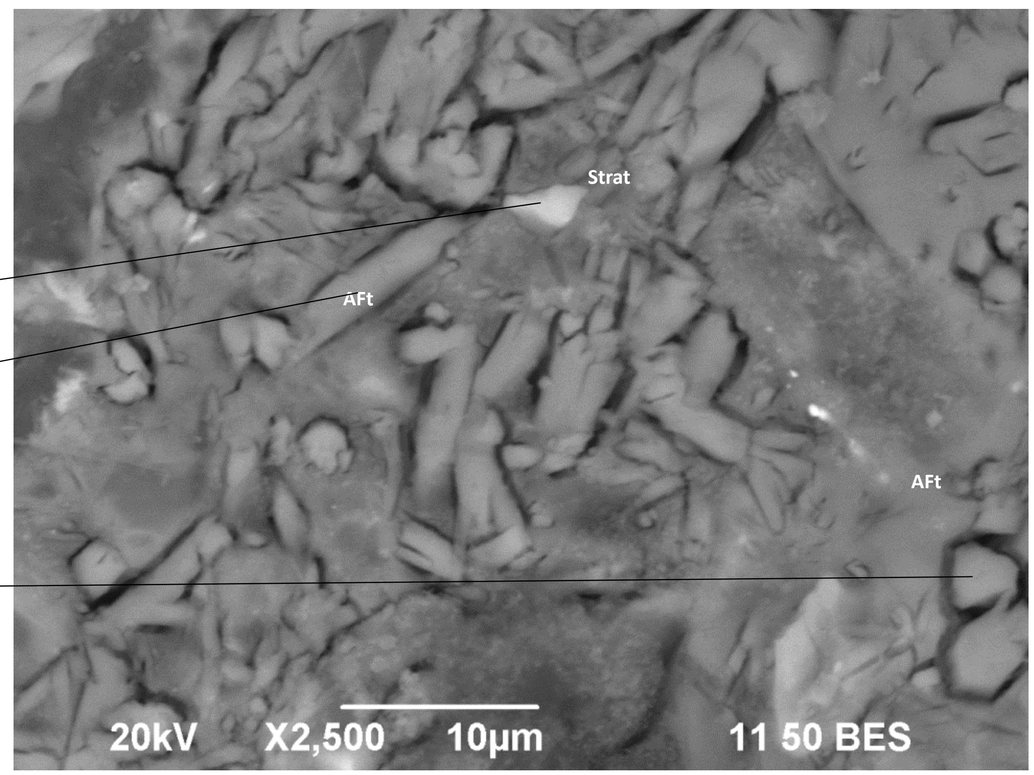

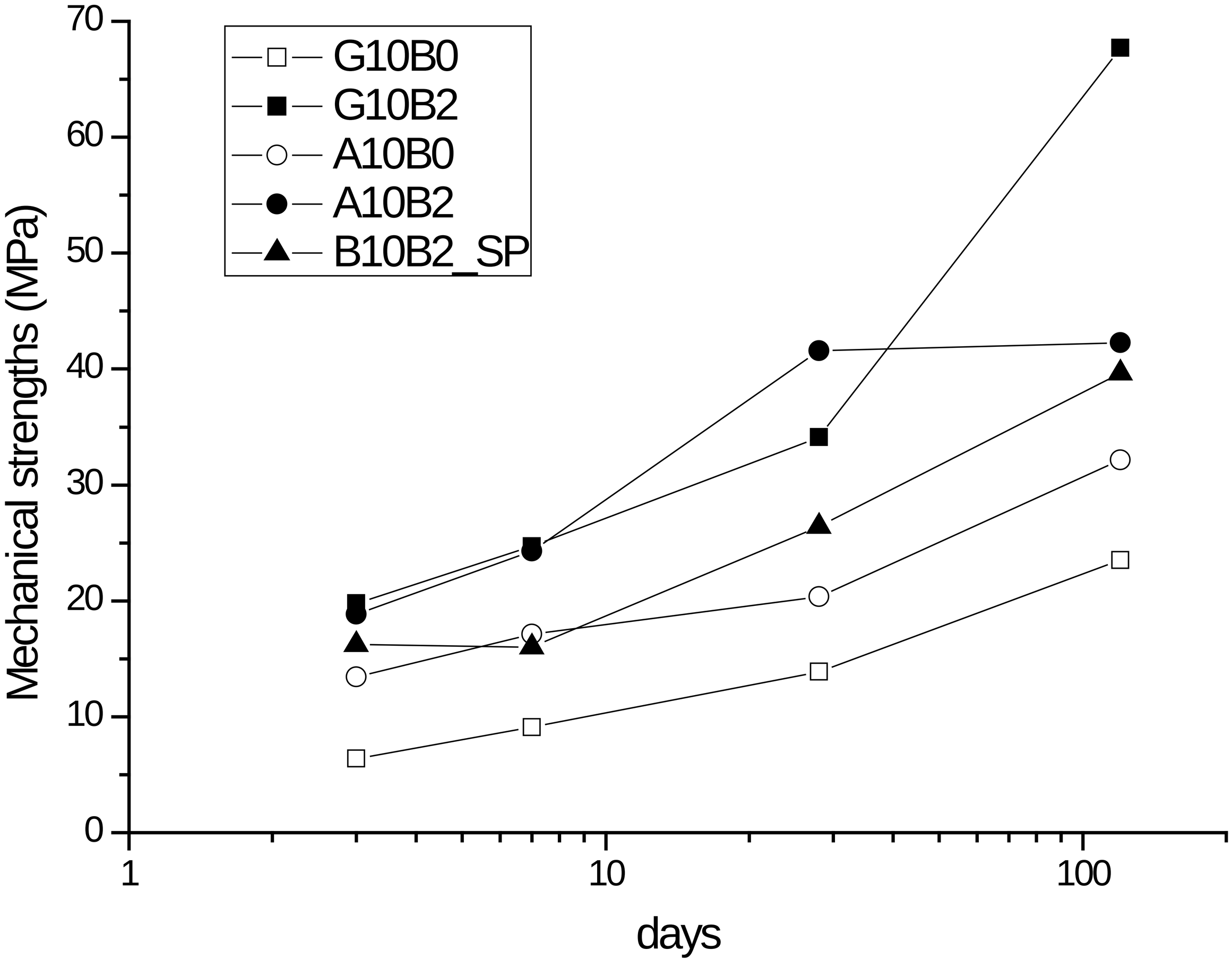
G10B0
G10B2
A10B0
A10B2
B10B2_SP
Mechanical strengths (MPa)
0
10
20
30
40
50
60
70
1
10
100
days